Nanoscale residual stress-field mapping around nanoindents in SiC by IR s-SNOM and confocal Raman microscopy

Alexander M. Gigler[1,3,*], Andreas J. Huber[2,3,4], Michael Bauer[1,3], Alexander Ziegler[4], Rainer Hillenbrand[2,3,5], and Robert W. Stark[1,3]

[1] *Department of Earth and Environmental Sciences, Ludwig-Maximilians-Universität München, Theresienstr. 41, 80333 Munich, Germany*
[2] *Nanooptics Laboratory, CIC nanoGUNE Consolider, 20018 Donostia – San Sebastian, Spain*
[3] *Center for NanoScience (CeNS), Schellingstr. 4, 80799 Munich, Germany*
[4] *Molekulare Strukturbiologie, Max-Planck-Insitut für Biochemie, 82152 Martinsried, Germany*
[5] *IKERBASQUE, Basque Foundation for Science*
**gigler@lmu.de*

Abstract: We map a nanoindent in a silicon carbide (SiC) crystal by infrared (IR) scattering-type scanning near-field optical microscopy (s-SNOM) and confocal Raman microscopy and interpret the resulting images in terms of local residual stress-fields. By comparing near-field IR and confocal Raman images, we find that the stress-induced shifts of the longitudinal optical phonon-frequencies (LO) and the related shift of the phonon-polariton near-field resonance give rise to Raman and s-SNOM image contrasts, respectively. We apply single-frequency IR s-SNOM for nanoscale resolved imaging of local stress-fields and confocal Raman microscopy to obtain the complete spectral information about stress-induced shifts of the phonon frequencies at diffraction limited spatial resolution. The spatial extension of the local stress-field around the nanoindent agrees well between both techniques. Our results demonstrate that both methods ideally complement each other, allowing for the detailed analysis of stress-fields at e.g. material and grain boundaries, in Micro-Electro-Mechanical-Systems (MEMS), or in engineered nanostructures.

©2009 Optical Society of America

OCIS codes: (180.4243) Near-field microscopy; (180.5655) Raman microscopy; (240.3695) Linear and nonlinear light scattering from surfaces; (240.5420) Polaritons; (240.6680) Surface plasmons; (300.6330) Spectroscopy, inelastic scattering including Raman

References and links

1. D. Peter, M. Dalmer, H. Kruwinus, A. Lechner, L. Archer, E. Gaulhofer, A. M. Gigler, R. W. Stark, and W. Bensch, "Measurement of the Mechanical Stability of Semiconductor Line Structures in Relevant Media," ECS Trans. **16**, 13–21 (2009).
2. I. Neizvestnyi, and V. Gridchin, "The use of stressed silicon in MOS transistors and CMOS structures," Russ. Microelectron. **38**(2), 71–86 (2009).
3. J. Baliga, *Silicon Carbide Power Devices* (World Scientific, Singapore, 2005).
4. H. Harima, T. Hosoda, and S. Nakashima, "Temperature measurement in a silicon carbide light emitting diode by Raman scattering," J. Electron. Mater. **28**(3), 141–143 (1999).
5. A. J. Wilkinson, G. Meaden, and D. J. Dingley, "High-resolution elastic strain measurement from electron backscatter diffraction patterns: new levels of sensitivity," Ultramicroscopy **106**(4-5), 307–313 (2006).
6. A. J. Wilkinson, G. Meaden, and D. J. Dingley, "Mapping strains at the nanoscale using electron back scatter diffraction," Superlattices Microstruct. **45**(4-5), 285–294 (2009).
7. M. Bauer, A. M. Gigler, A. J. Huber, R. Hillenbrand, and R. W. Stark, "Temperature depending Raman line-shift in silicon carbide," J. Raman Spectrosc. (to be published)), doi:10.1002/jrs.2334.
8. M. Bauer, A. M. Gigler, C. Richter, and R. W. Stark, "Visualizing stress in silicon micro cantilevers using scanning confocal Raman spectroscopy," Microelectron. Eng. **85**(5-6), 1443–1446 (2008).
9. T. Beechem, S. Graham, S. P. Kearney, L. M. Phinney, and J. R. Serrano, "Invited Article: Simultaneous mapping of temperature and stress in microdevices using micro-Raman spectroscopy," Rev. Sci. Instrum. **78**(6), 061301 (2007).

#117434 - $15.00 USD Received 18 Sep 2009; revised 26 Oct 2009; accepted 9 Nov 2009; published 23 Nov 2009

10. D. Olego, M. Cardona, and P. Vogl, "Pressure-Dependence of the Optical Phonons and Transverse Effective Charge in 3C-SiC," Phys. Rev. B **25**(6), 3878–3888 (1982).
11. H. F. Poulsen, J. A. Wert, J. Neuefeind, V. Honkimäki, and M. Daymond, "Measuring strain distributions in amorphous materials," Nat. Mater. **4**(1), 33–36 (2005).
12. A. Debernardi, C. Ulrich, K. Syassen, and M. Cardona, "Raman linewidths of optical phonons in 3C-SiC under pressure: First-principles calculations and experimental results," Phys. Rev. B **59**(10), 6774–6783 (1999).
13. T. B. Wei, Q. Hu, R. F. Duan, J. X. Wang, Y. P. Zeng, J. M. Li, Y. Yang, and Y. L. Liu, "Mechanical Deformation Behavior of Nonpolar GaN Thick Films by Berkovich Nanoindentation," Nanoscale Res. Lett. **4**(7), 753–757 (2009).
14. J. C. Burton, L. Sun, M. Pophristic, S. J. Lukacs, F. H. Long, Z. C. Feng, and I. T. Ferguson, "Spatial characterization of doped SiC wafers by Raman spectroscopy," J. Appl. Phys. **84**(11), 6268–6273 (1998).
15. S. Nakashima, and H. Harima, "Raman investigation of SiC polytypes," Phys. Status Solidi A **162**(1), 39–64 (1997).
16. K. Mizoguchi, and S. Nakashima, "Determination of Crystallographic Orientations in Silicon Films by Raman-Microprobe Polarization Measurements," J. Appl. Phys. **65**(7), 2583–2590 (1989).
17. I. DeWolf, "Micro-Raman spectroscopy to study local mechanical stress in silicon integrated circuits," Semicond. Sci. Technol. **11**(2), 139–154 (1996).
18. S. M. Hu, "Stress-Related Problems in Silicon Technology," J. Appl. Phys. **70**(6), R53–R80 (1991).
19. B. V. Kamenev, H. Grebel, L. Tsybeskov, T. I. Kamins, R. S. Williams, J. M. Baribeau, and D. J. Lockwood, "Polarized Raman scattering and localized embedded strain in self-organized Si/Ge nanostructures," Appl. Phys. Lett. **83**(24), 5035–5037 (2003).
20. J. Liu, and Y. K. Vohra, "Raman modes of 6H polytype of silicon carbide to ultrahigh pressures: A comparison with silicon and diamond," Phys. Rev. Lett. **72**(26), 4105–4108 (1994).
21. J. Liu, and Y. K. Vohra, "Raman modes of 6H polytype of silicon carbide to ultrahigh pressures - Reply," Phys. Rev. Lett. **77**, 1661 (1996).
22. L. G. Cançado, A. Hartschuh, and L. Novotny, "Tip-enhanced Raman spectroscopy of carbon nanotubes," J. Raman Spectrosc. **40**(10), 1420–1426 (2009).
23. A. Hartschuh, E. J. Sánchez, X. S. Xie, and L. Novotny, "High-resolution near-field Raman microscopy of single-walled carbon nanotubes," Phys. Rev. Lett. **90**(9), 095503 (2003).
24. D. Cialla, T. Deckert-Gaudig, C. Budich, M. Laue, R. Moller, D. Naumann, V. Deckert, and J. Popp, "Raman to the limit: tip-enhanced Raman spectroscopic investigations of a single tobacco mosaic virus," J. Raman Spectrosc. **40**(3), 240–243 (2009).
25. T. Deckert-Gaudig, F. Erver, and V. Deckert, "Transparent silver microcrystals: synthesis and application for nanoscale analysis," Langmuir **25**(11), 6032–6034 (2009).
26. T. Deckert-Gaudig, E. Bailo, and V. Deckert, "Perspectives for spatially resolved molecular spectroscopy - Raman on the nanometer scale," J. Biophoton. **1**(5), 377–389 (2008).
27. N. Hayazawa, M. Motohashi, Y. Saito, H. Ishitobi, A. Ono, T. Ichimura, P. Verma, and S. Kawata, "Visualization of localized strain of a crystalline thin layer at the nanoscale by tip-enhanced Raman spectroscopy and microscopy," J. Raman Spectrosc. **38**(6), 684–696 (2007).
28. A. Tarun, N. Hayazawa, M. Motohashi, and S. Kawata, "Highly efficient tip-enhanced Raman spectroscopy and microscopy of strained silicon," Rev. Sci. Instrum. **79**(1), 013706 (2008).
29. F. Keilmann, and R. Hillenbrand, "Near-field microscopy by elastic light scattering from a tip," Philos. Trans. R. Soc. Lond. A **362**(1817), 787–805 (2004).
30. R. Hillenbrand, T. Taubner, and F. Keilmann, "Phonon-enhanced light matter interaction at the nanometre scale," Nature **418**(6894), 159–162 (2002).
31. S. C. Kehr, M. Cebula, O. Mieth, T. Härtling, J. Seidel, S. Grafström, L. M. Eng, S. Winnerl, D. Stehr, and M. Helm, "Anisotropy contrast in phonon-enhanced apertureless near-field microscopy using a free-electron laser," Phys. Rev. Lett. **100**(25), 256403 (2008).
32. A. Huber, N. Ocelic, T. Taubner, and R. Hillenbrand, "Nanoscale resolved infrared probing of crystal structure and of plasmon-phonon coupling," Nano Lett. **6**(4), 774–778 (2006).
33. N. Ocelic, and R. Hillenbrand, "Subwavelength-scale tailoring of surface phonon polaritons by focused ion-beam implantation," Nat. Mater. **3**(9), 606–609 (2004).
34. A. J. Huber, A. Ziegler, T. Köck, and R. Hillenbrand, "Infrared nanoscopy of strained semiconductors," Nat. Nanotechnol. **4**(3), 153–157 (2009).
35. N. Ocelic, A. Huber, and R. Hillenbrand, "Pseudoheterodyne detection for background-free near-field spectroscopy," Appl. Phys. Lett. **89**(10), 101124 (2006).
36. U. Schmidt, W. Ibach, J. Muller, K. Weishaupt, and O. Hollricher, "Raman spectral imaging - A nondestructive, high resolution analysis technique for local stress measurements in silicon," Vib. Spectrosc. **42**(1), 93–97 (2006).
37. T. Wermelinger, C. Borgia, C. Solenthaler, and R. Spolenak, "3-D Raman spectroscopy measurements of the symmetry of residual stress fields in plastically deformed sapphire crystals," Acta Mater. **55**(14), 4657–4665 (2007).
38. G. D. Quinn, and R. C. Bradt, "On the Vickers indentation fracture toughness test," J. Am. Ceram. Soc. **90**(3), 673–680 (2007).
39. M. Becker, H. Scheel, S. Christiansen, and H. P. Strunk, "Grain orientation, texture, and internal stress optically evaluated by micro-Raman spectroscopy," J. Appl. Phys. **101**(6), 063531 (2007).

#117434 - $15.00 USD Received 18 Sep 2009; revised 26 Oct 2009; accepted 9 Nov 2009; published 23 Nov 2009
(C) 2009 OSA

1. Introduction

Mechanical and residual strain in semiconductor materials play an important role in the design of devices. For example, strain can give rise to failure, in particular due to the collapse of high aspect-ratio features [1]. Controlled strain engineering, however, allows affecting free carrier mobility in semiconductors and may enable manipulation and customization of novel electronic devices at the nano-scale [2]. One of the more robust semiconductor materials is silicon carbide (SiC). It is used in demanding applications under elevated temperatures, high voltage, and for optical applications in the ultra violet region [3,4]. Thus, local strain measurements are necessary for monitoring and optimization of fabrication processes. For this purpose, it is desirable to use non-invasive and fast techniques for strain mapping that require only minimum sample preparation. Precise local strain measurements can be, for example, achieved by electron backscatter diffraction [5,6]. For routine analysis, however, optical methods are desirable because they require less preparation. As the frequency of phonon modes is changing under external influences such as mechanical stress and strain [7–13], both infrared near-field microscopy and Raman spectroscopy are well suited techniques.

Raman scattering in SiC occurs on longitudinal and transversal acoustic (LA, TA) and on optical (LO, TO) phonon modes. Scattering at folded modes can occur in higher order SiC polytypes due to the increased size of the unit cell [14,15]. The orientation of the crystal axes with respect to the actual polarization of the incident laser, can cause anisotropic Raman scattering signals [16]. Together with the strain tensor, the effect of polarization has been investigated for silicon [17,18] and silicon-germanium nanostructures [19]. Raman spectroscopy is highly sensitive to variations in phonon frequencies, i.e. the line shift. These variations can be caused by modifications of the equilibrium distance between atoms due to either mechanical stress or changing temperature [9]. Because the peak width is mainly depending on the sample temperature, whereas the peak position is affected by both stress and temperature, these effects can be separated. However, high mechanical stress [20,21] as well as defects may also influence the line width [17]. In general, not only external influences but also intrinsic effects of the measurement process, such as the strongly focused laser, can cause heating of the sample and – in turn – line shifts. In the case of SiC, however, such a local heating effect can be excluded for moderate laser intensities, because the absorption coefficient of SiC (1.59 per cm at 532 nm) is very small and the penetration depth is about 2 mm [7]. Hence, confocal Raman spectroscopy enables a direct measurement of the local distribution of mechanical stress and strain in SiC samples with a lateral resolution determined by the confocal spot size.

Confocal techniques are limited by diffraction. The diffraction limit can be overcome by optical near-field techniques. For example, tip-enhanced Raman spectroscopy can provide a sub-wavelength lateral resolution [22–28]. Another highly resolving spectroscopic technique is scattering-type scanning near-field optical microscopy (s-SNOM) [29]. At infrared frequencies, s-SNOM can probe the structural properties of infrared-active materials such as SiC, SiN, SiO, GaN, or GaAs with nanometer resolution. In s-SNOM the metalized tip of an Atomic Force Microscope (AFM) is illuminated by laser light. The concentrated optical fields at the tip apex can excite localized surface phonon-polaritons (optical lattice vibrations), yielding a near-field resonance at a material specific frequency ω_{sp} close to the LO phonon frequency [30,31]. As the phonon frequencies strongly depend on the crystal lattice, spectroscopic recording of the backscattered infrared radiation allows for nano-scale mapping of polytypism [32], crystal quality [33], or anisotropy [31]. The surface phonon-polariton near-field resonance of SiC also varies with compressive or tensile strain, which enables imaging of strain-fields [34].

Here, we use confocal Raman microscopy to map the stress-fields introduced in a 6H-SiC sample by means of nanoindentation. We focus on the stress-induced line shifts of the TO and LO phonon modes of the sample. In addition we compare our results to s-SNOM measurements of the identical nanoindent. Our study shows that confocal Raman microscopy and s-SNOM probe the direct effects of stress on the phonon spectrum of the sample.

#117434 - $15.00 USD Received 18 Sep 2009; revised 26 Oct 2009; accepted 9 Nov 2009; published 23 Nov 2009
(C) 2009 OSA

The differences in axial resolution and, thus, image contrast formation are discussed in the following. Furthermore, we demonstrate the high-resolution capabilities of s-SNOM, revealing nanocracks at a resolution far beyond the diffraction limit of a confocal Raman microscope. The combination of both analytic techniques proves highly effective for the assessment of local stress distributions with full spectral information as well as high resolution data at a single frequency.

2. Materials and methods

We investigated the hexagonal polytype of silicon carbide (6H-SiC). The sample was a single crystal of 6H-SiC with (0001) orientation polished to epitaxy-ready grade. Due to the hexagonal symmetry of the 6H-SiC crystal and the (0001) orientation of the crystallographic axis, the s-SNOM contrast is independent of the illumination direction for the given experimental setup. To generate local stress fields at the surface of the SiC crystal, a NanoTest 600 (Micro Materials Ltd.) device equipped with a pyramidal indenter (Berkovich) was used. The loading and unloading rate for the indentation was 0.5 mN/s, while the force was held constant at maximum load for 5 s. The nanoindentations were created with a maximum load of 50 mN resulting in 130 nm deep elasto-plastic deformations (triangular depressions). The identical indent was examined by both confocal Raman microscopy and s-SNOM.

Raman spectra were recorded by a confocal Raman microscope (alpha300 R; WITec GmbH, Ulm, Germany). The system was equipped with a SHG Nd:YAG laser (532 nm, 22.5 mW) and a lens-based spectrometer. Elastically scattered photons were rejected by a sharp edge filter. With a 1800 mm^{-1} grating, the spectral resolution was 1.17 cm^{-1} per CCD-pixel. The Raman peaks were fitted with a Lorentzian profile. Spectra were recorded at each image pixel with an integration time of 0.4 s. Due to the band-gap of 3.0 eV for 6H-SiC compared to the photon energy of 2.33 eV, the scattering process was non-resonant. A 100 × microscope objective (working distance 0.26 mm, NA 0.90) was used for the measurements. Due to the holographic beam splitter, the incident light was polarized along the x-axis of the scan. However, our measurements can be regarded as “unpolarized”, because no analyzer was used. Thus, a stress magnitude is measured rather than the exact components of the strain tensor. The diffraction limited focus resulted in a lateral resolution of about 400 nm. A multimode optical fiber guided the signal to the spectrometer. The 50-µm-core of this fiber was used as confocal pinhole leading to an axial focal depth of about 1 µm.

The scattering-type scanning near-field optical microscope (s-SNOM) used for this work is based on a custom-built atomic force microscope (AFM). The technical details have been reported elsewhere [30,32–35]. In this setup, the metalized tip of an AFM cantilever is illuminated by a frequency-tunable CO_2 laser providing wavelengths between ω_{IR} = 887 cm^{-1} and ω_{IR} = 1085 cm^{-1} (λ_{IR} = 9.21 µm – 11.27 µm). The backscattered light was recorded simultaneously with topography providing ultra-high resolution infrared near-field images.

3. Result and discussion

The peaks in the Raman spectra of unstressed SiC were identified and assigned to the phonon lines of 6H-SiC according to literature [15]: 234.6 cm^{-1} (folded TA-planar), 240.0 cm^{-1} (FTA-planar), 505.5 cm^{-1} (FLA-axial), 787.9 cm^{-1} (FTO-planar), 798.0 cm^{-1} (FTO-planar), 889.3 cm^{-1} (TO-planar), and 971.5 cm^{-1} (LO-axial). In the following, we discuss the optical phonon-lines (ω_{TO} = 889.3 cm^{-1} and ω_{LO} = 971.5 cm^{-1}). Figure 1 shows the Raman spectrum of 6H-SiC in the region of optical phonons (ω = 775 cm^{-1} – 990 cm^{-1}). The inset shows the change in the spectra for different loading conditions taken from different regions around the indent. The green curve indicates the position and curve shape of the TO and LO peaks obtained for the unstressed material. With respect to the excitation wavelength, the peaks are shifted to lower wavenumbers for tensile stress, while for compressive stress they are shifted to higher values. In analogy to Liu and Vohra’s work [20,21], we can estimate a maximal mechanical stress around the indent of about ± 1 GPa from the line-shift of about ± 2 cm^{-1}.

#117434 - $15.00 USD Received 18 Sep 2009; revised 26 Oct 2009; accepted 9 Nov 2009; published 23 Nov 2009
(C) 2009 OSA

This conclusion is supported by the increasing separation of the TO and LO center frequencies with increasing pressure, yielding a similar value for the stress magnitude.

Note that the precise calculation of the local stress and strain from the shift of the phonon frequencies depends on crystal orientation and polarization of the incident light. As our measurements were unpolarized, the local stress obtained here corresponds to a scalar average rather than exact components of the strain tensor.

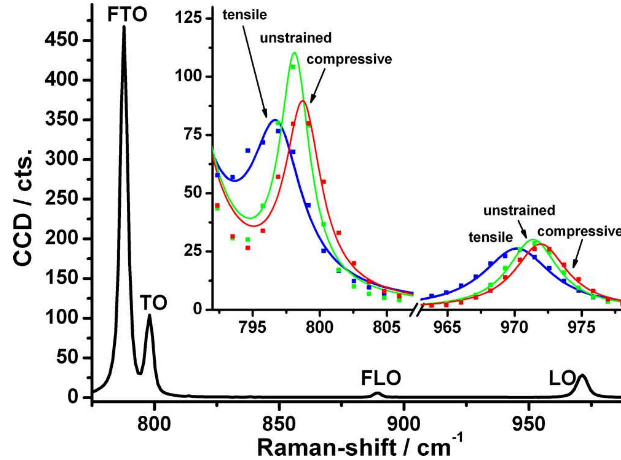

Fig. 1. (color online): Typical Raman spectrum of unstressed 6H-SiC of the most prominent phonon lines at 889.3 cm^{-1} (TO-planar) and 971.5 cm^{-1} (LO-axial). The inset shows the TO and LO peaks under tensile (blue), neutral (green), and compressive (red) loading causing corresponding line-shifts and line-broadening (symbols: experiment; lines: Lorentzian fit).

We examined the identical indent in both Raman and s-SNOM measurements (Fig. 2). All images in Fig. 2 show a 15 µm × 15 µm scan field. A map of the elastically scattered intensity (Rayleigh scattering) recorded at diffraction limited spatial resolution by the confocal Raman microscope is shown in Fig. 2(a). Regions of interest were labeled A-D. In order to obtain stress-distribution images from the Raman spectral data, the phonon lines were fitted by Lorentzian profiles and the center frequencies (Figs. 2(b) and 2(c)) of the peaks were determined for each pixel. The center frequencies were shifted to higher wavenumbers where compressive stress was present (close to the edges of the indent) and to lower wavenumbers where tensile stress occurred (corners of the indent) [36]. The maximum shift amounts to about ± 2 cm^{-1} for the TO and LO phonons. As seen in Figs. 2(b) and 2(c), compressive stress was induced in regions A and C, while in the regions B and D near the indent mainly tensile stress occurred. In Figs. 2(b) and 2(c) the stress field around the indent is not perfectly symmetric. The asymmetry of the stress pattern, i.e. that we find tensile stress instead of compression at position D, we explain by a slight misalignment of the indenter, i.e. the indentation was not performed perfectly perpendicular to the sample surface. In addition, due to the axial focus of approximately 1 µm, not only the topmost stressed surface of the SiC sample was probed, but also stress distributions beneath the surface of the crystal can contribute to the spectra. Thus, an effective stress, i.e. an average stress of the sampled depth, was measured rather than one highly localized at the surface.

Figures 2(d) - 2(f) show s-SNOM images of the indent in 6H-SiC. The triangular depression of 130 nm depth is located in the center of the topography image (Fig. 2(d)). The topography image does not reveal any stress-related features. In the infrared near-field images (Figs. 2(e) and 2(f)), strong contrasts can be observed in the proximity of the indent. The near-field contrast reveals the characteristic pattern of residual stress-fields as detected in the confocal Raman images (see Figs. 2(b) and 2(c)), yet at much higher spatial resolution. In the near-field image recorded at ω_{IR} = 924 cm^{-1}, regions near the edges of the indent appear in dark and near the corners in bright contrast as compared to the undisturbed surface region.

#117434 - $15.00 USD Received 18 Sep 2009; revised 26 Oct 2009; accepted 9 Nov 2009; published 23 Nov 2009
(C) 2009 OSA

This contrast sequence is reversed for ω_{IR} = 944 cm^{-1}. The inversion of the image contrast is due to the fact that the s-SNOM images are recorded at single frequencies, slightly below and above the resonance frequency of the surface phonon-polariton near-field resonance [32].

The amplitude contrast of the s-SNOM images of the indent can be assigned to stress-induced shifts of this surface phonon-polariton near-field resonance. The s-SNOM images reveal compressive stress at the edges of the indent and tensile stress at its corners [34].

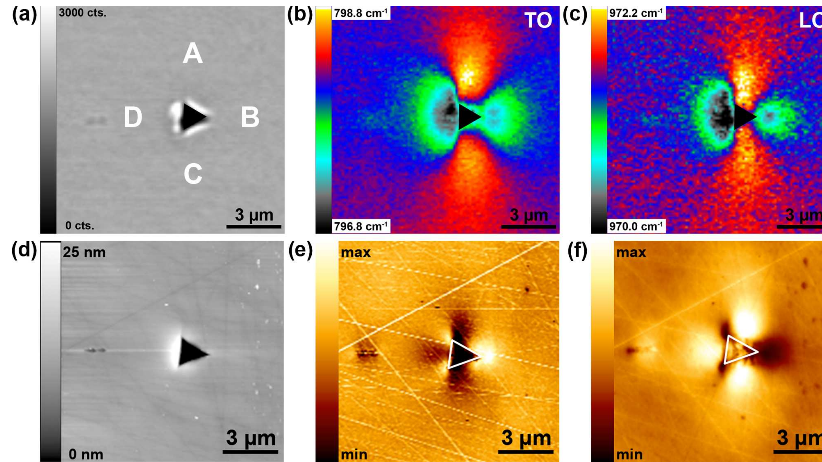

Fig. 2. (color online): Confocal Raman microscopy and s-SNOM images of a locally stressed SiC sample. (a) Rayleigh intensity map. Four regions of interest are labeled A-D, (b, c) maps of the spectral position of the fitted TO and LO phonon lines as obtained by fitting a Lorentzian. Black triangles mark the contour of the indent. For comparison, s-SNOM amplitude maps of the identical indent are given in (d-f). (d) Shows the topography of the indent, (e) s-SNOM amplitude detected for ω_{IR} = 924 cm^{-1} and (f) ω_{IR} = 944 cm^{-1} laser frequencies reveal the characteristic amplitude contrasts around the indent. Note that in the near-field optical images the scratches exhibit a pronounced contrast, which can be explained by crystal damage caused by the mechanical polishing process [33].

Comparison of the confocal Raman maps and the IR near-field images of the indent reveals that both methods exhibit stress-induced contrasts around the nanoindent caused by the indentation process. The spatial extension and geometry of the lobes around the indent agree well between the confocal Raman and the IR s-SNOM images. A deviation between near-field s-SNOM and confocal Raman maps was found in Figs. 2(b), 2(c), 2(e), and 2(f) at the position D of the indent. In the s-SNOM images, highly localized tensile stress-fields were identified at the corners in region D of the indent as well as a larger compressively stressed sample area at position D. The confocal Raman images, on the other hand, revealed only tensile stress for this specific sample area. In order to understand the differences in image contrast formation at region D, two effects have to be considered. First, while s-SNOM probes the very surface of the sample, confocal Raman scattering occurs within surface-near layers up to several 100 nm beneath the surface. Due to the averaging over the entire confocal volume, the signal of Raman scattering was dominated by the differently stressed material deeper inside the 6H-SiC crystal. Such an averaging effect has also been observed by Wermelinger *et al.* for a Vickers indentation in GaN [37]. Second, the confocal Raman microscopy images reveal how stress affects the in-plane (parallel to sample surface) TO and LO phonon frequencies. In s-SNOM, the probing infrared field at the tip apex is largely depolarized, thus probing stress-induced changes of the phonon polaritons both parallel and perpendicular to the sample surface. Because of the slightly misaligned indenter, we can assume that the stress distributions perpendicular and parallel to the sample surface differ from each other, yielding the differences in the stress patterns observed by confocal Raman and s-SNOM images.

#117434 - $15.00 USD Received 18 Sep 2009; revised 26 Oct 2009; accepted 9 Nov 2009; published 23 Nov 2009
(C) 2009 OSA

The potential of infrared s-SNOM for the mapping of nano-scale stress-fields is demonstrated by imaging a corner of the indent at higher resolution as shown in the topography image in Fig. 3(a). The corresponding amplitude image (Fig. 3(b)) recorded at ω_{IR} = 935 cm^{-1} clearly reveals a dark line emanating from the corner of the indent (corresponding to position B in Fig. 2(a)) with a circular shaped contrast at its end.

Congruent results of finite element calculations and macroscopic investigations of similar configurations confirm, that at such critical edge locations of indents where tensile stress occurs, formation of such cracks is preferential [38]. The bulb-shaped feature observed at the end of the dark line, exhibits an amplitude contrast of a tensile stressed sample area, which is characteristic for the stress-field at crack tips [36,39]. The dark line, thus, corresponds to the signature of the nanocrack. Indeed, the topography at an even smaller scan range reveals also a small crack in the sample surface.

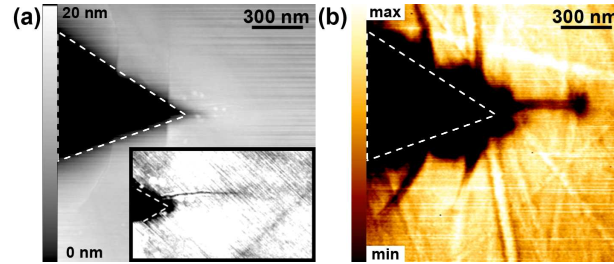

Fig. 3. (color online): s-SNOM hardware zoom into the right corner of the indent revealing a nanocrack emanating from the edge. (a) Topography and (b) s-SNOM amplitude at ω_{IR} = 935 cm^{-1}. The inset in (a) shows an additional hardware-zoom of the corner of the indent revealing a nanocrack in the topography data.

4. Conclusion

In summary we have shown that confocal Raman microscopy and s-SNOM imaging reveal a qualitative contrast of the stress-fields around nanoindentation sites. Both data sets correspond in their spatial extension. The resolution of the methods differs considerably, s-SNOM being approximately 10-20 times better. The shift of the phonon frequencies as probed by Raman scattering can be directly related to local stress similarly as it was detected for the near-field phonon-polariton resonance. The magnitude of the phonon line shift agrees well with the shift of the phonon-polariton near-field resonance. Thus, based on the near-field scattering intensity of a single selected wavelength, s-SNOM allows to resolve the smallest features of the indent down to nanocracks while diffraction limited confocal Raman spectroscopy gives the full spectral information of the changes in phonon dispersion. Scattering-SNOM is sensitive to the stress distribution near the surface, while far-field Raman scattering also occurs beneath the surface and can reveal changes in sub-surface stress distributions.

Acknowledgements

We thank the DFG cluster of excellence “Nanosystems Initiative Munich” (NIM) for financial support.

#117434 - $15.00 USD Received 18 Sep 2009; revised 26 Oct 2009; accepted 9 Nov 2009; published 23 Nov 2009
(C) 2009 OSA